Investigating the use of quantum solvers for simulating classical systems

Andrew Eberhardt, Arka Banerjee, Michael Kopp, and Tom Abel
Kavli Institute for Particle Astrophysics and Cosmology, Menlo Park, 94025, CA
Physics Department, Stanford University, Stanford, CA and
SLAC National Accelerator Laboratory

We explore how closely Schrödinger–Poisson system of equations can model the classical Vlasov–Poisson system in one and two dimensions. We consider gravitational collapse problems as well as the electrostatic plasma case where the constant in the Poisson equation is of opposite sign. We discuss the bump on tail problems, Landau damping, the two stream instability, as well as cold and warm gravitational collapse problems. We also describe a code that solves the density matrix formalism and demonstrate how it can evolve initial conditions that are not a pure state as required by the typical Schrödinger-Poisson system.

I. INTRODUCTION

Quantum solvers have proved useful for simulating a number of physical phenomena. These solvers have been applied to study two distinct types of systems. The first are those systems in which the quantum nature of the constituents is relevant, such as fuzzy dark matter [1–11], quantum plasmas [12], and small electronics [13, 14]. The second type are systems where the quantum solver approximates the classical solution, such as cold dark matter [7, 11, 15–20] and classical plasmas [21–24]. One motivation in the latter application is to map out and understand the regimes of correspondence between quantum solvers and traditional classical methods [7, 13, 15–18, 21–23]. This correspondence is of particular interest because of quantum solvers' potential ability to reduce the computational resources necessary to simulate certain systems [11, 13, 15, 17] as well as circumvent some of the problems associated with classical solvers [7].

The most commonly used quantum solver, i.e. the Schrödinger-Poisson method, at the most basic level, evolves an array of complex numbers in time using the Schrödinger Poisson equations. This array can be thought of as representing a "wavefunction" in some basis, but is more often interpreted as a complex classical field [17]. As with true quantum wavefunctions however, one can interpret the square of the absolute value of a given element as the probability density at that position in the chosen basis, typically the position or velocity bases [15]. In the limit of a large number of particles, as in classical systems, this probability density corresponds to a density. Further, the derivative of the phase of the complex number can be interpreted as a position of that density in the reciprocal space of the basis. For example, when represented in the position basis, the derivative of the phase corresponds to the velocity of the stream at that position [17]. This wavefunction is advanced in time using the Schrödinger equation, where the potential term appearing in the equation is computed using the Poisson equation – where the density is given by the square of the absolute value of the wavefunction in the position basis [17]. Note that Fourier transforms relate position and momentum spaces, allowing the wavefunction, and by extension, the quantum solver methods, to represent both spatial density, as well as velocity dispersion [15]. An approximation of a classical phase space representation can then be created with the Husimi transform [7, 15, 17, 18, 25], allowing a full description of our system.

Investigation of the classical limit of these solvers has been a topic of active research in the literature for some time [7, 13, 15–18, 21–23]. The specific way in which the solutions from the quantum solvers reduce to the classical limit, as well as the limitation and benefits of using these solvers in quantum scenarios is not fully understood, but it has been shown that quantum methods are quite successful in simulating some classical plasma problems involving cold initial conditions [12, 13, 15, 17].

When used as approximations of classical systems, quantum solvers presents a scenario which a $2 \times n$ dimensional phase space can be represented by an n dimensional array of complex numbers [7, 15, 17]. This means that for appropriate systems, the quantum representation may use fewer computational resources. Many of the systems which are interesting to simulate in physics require a large amount of computational resources, and so understanding the limitations and benefits of quantum solvers may provide new means to investigate these systems via simulation. Further, classical methods are known to exhibit shot noise in low density regions [7]. Quantum techniques which use continuous fields can, in principle, circumvent this problem [7].

In this work we investigate the quantum solvers' correspondence with classical solver by looking at the results of a number of test problems. We discuss both how the classical limit is achieved, as well as the cause of the deviation. We demonstrate that separation of streams in phase space is necessary to approximate the classical solutions using the standard Schrödinger method. Importantly, we show that the limit of validity can be extended to warm initial conditions, in which streams may be poorly resolved, by using modifications to this technique.

We layout the paper as follows. Section II contains a description of each solver used in the paper including a description of how to create initial conditions, the solver update rule, and discussion of how quantum solvers correspond to classical counterparts. In Section III we discuss how to transform our quantum representations into phase space representations. Section IV contains a series of test cases in which we investigate the ability of quantum solvers to reproduce classical results. We include a discussion of the results in Section V. Conclusions are presented in Section VI.

II. SOLVERS

In this section, we discuss the different methods explored in this paper, including the procedures for setting up consistent initial conditions for the different solvers, along with the update rules for the variables of each method. For the quantum solvers, we also discuss the conditions under which these solvers correspond to the solution of the classical Vlasov-Poisson system, along with the conditions under which they deviate from the classical solution. The code units are discussed in the Appendix . All solvers use a kick-drift-kick update scheme that works as follows:

1. half step position update
2. calculate potential
3. full step momentum update
4. half step position update

A. Classical Solver

1. *Initial conditions*

For the classical solver, the system is discretized in terms of particles. We generate initial conditions for this solver simply by choosing an initial position and velocity for each particle, sampled from the initial distribution function. We first divide up the total number of particles $N_{\rm part}$ into individual streams. The streams are populated with particles according to their Boltzmann weights i.e. the number of particles in the ith stream is

$$N^i_{\rm part} = N_{\rm part}\frac{e^{-v_i^2/v_{th}^2}}{Z}\,, \tag{1}$$

where $N^i_{\rm part}$ is the total number of particles in stream i, v_i is the mean velocity of the stream, and v_{th} is the thermal velocity. Z is the partition function of the system defined as

$$Z = \sum_i e^{-v_i^2/v_{th}^2}\,. \tag{2}$$

To determine the position of particles within a given stream, we compute the Cumulative Distribution Function (CDF) of the initial density distribution:

$$\mathrm{CDF}(r) \equiv \int_{-\infty}^{r} \rho(\tilde{r})d\tilde{r}\,. \tag{3}$$

The position for the j-th particle in the stream can be found by inverting this CDF, i.e. the particle is assigned position r_j which satisfies

$$\mathrm{CDF}(r)|_{r=r_j} = \frac{j+1}{N^i_{\rm part}+2}\,. \tag{4}$$

For the plasma simulations, the initial spatial density is constant and so this procedure implies that the particles are spaced uniformly over the simulation length. Finally, the velocity for particle j, starting in stream i is assigned as follows

$$v_j = v_i + v_p \sin\left(2\pi\frac{r_j}{\lambda}\right) \tag{5}$$

where v_p controls the magnitude of the perturbation of velocity about the mean velocity v_i of the stream.

2. *Update*

Once the initial conditions have been set up, we have two arrays of length $N_{\rm part}$ representing the positions and velocities which need to be updated at every time step. The update rule is described in Table I.

The accelerations, a, are computed as follows: the particle positions are used to create a density field

	classical	Schrödinger	multiple Hilbert spaces	Von Neumann
position	$r_{t+\Delta t} = r_t + v\,\Delta t$	$\tilde{\psi}_{t+\Delta t} = U_T(\Delta t)\tilde{\psi}_t$	$\tilde{\psi}_{t+\Delta t,i} = U_T(\Delta t)\tilde{\psi}_{t,i}$	$\tilde{P}_{t+\Delta t} = U_T(\Delta t)U_T^\dagger(\Delta t)\tilde{P}_t$
momentum	$v_{t+\Delta t} = v_t + a\,\Delta t$	$\psi_{t+\Delta t} = U_V(\Delta t)\psi_t$	$\psi_{t+\Delta t,i} = U_V(\Delta t)\psi_{t,i}$	$P_{t+\Delta t} = U_V(\Delta t)U_V^\dagger(\Delta t)P_t$
density	CIC deposit	$\lvert\psi\rvert^2$	$\sum_{i=1}^{N_s}\lvert\Psi_i\rvert^2$	diag(P)

TABLE I. Shown for each solver is the full step position update, momentum update, and density deposit rules.

$\rho(r)$ using the Paricle-in-Cell deposition schemes. The computation of the acceleration from the density field is done in Fourier space, so we consider the Fourier transform of the density:

$$\tilde{\rho}(k) = \int \rho(r) e^{ikr} dr\,. \tag{6}$$

In Fourier space, the Poisson equation has a particularly simple form, and the potential is calculated as:

$$\tilde{V}(k) = -\frac{C}{(2\pi)^2}\frac{\tilde{\rho}(k)}{k^2}\,. \tag{7}$$

The potential is then tranformed back to configuration space:

$$V(r) = \frac{1}{2\pi}\int \tilde{V}(k) e^{-ikr} dk\,, \tag{8}$$

and finally the acceleration is computed as $a = -D\,V(r)$ where D represents the differentiation stencil. While the above expressions have been written for continuous fields for conceptual clarity, the actual calculations are performed on a grid of size $N_{\rm grid}$ using Discrete Fourier Transforms. The acceleration is then interpolated back to the particle positions to perform the velocity update. Apart from the computation of the acceleration in the final step, the procedure of going from the density field to the potential as outlined above is also used for all the other solvers that are described below.

B. Schrödinger–Poisson solver

In the language of quantum mechanics the implicit assumption contained in the Schrödinger-Poisson solver is that the evolved wave function correspond to a pure state. This means that streams are added in superposition as opposed to being in a classical statistical mixture. As we will explore further in the later sections, in using this method as an alternative to a classical solver, we choose to interpret the wave function densities as corresponding to classical distribution functions but the solver itself allows for wave mechanic effects like interference that would not be present in the classical solution. When using this solver to approximate classical solutions it should be noted that $\hbar$ is not the physical constant but a simulation parameter representing a minimum phase space resolution [16]. We will discuss in more detail how $\hbar$ relates to the deviation from the classical solution in II B 3.

1. *Initial conditions*

We generate the initial conditions of this solver by populating our phase space with streams represented by a single one (spatial) dimensional wavefunction defined on a grid with $N_{\rm grid}$ cells. The wavefunction can be represented in the following way in either configuration space or momentum space:

$$\psi(x) = \sqrt{\rho}\exp\left(i\phi\right)\,, \tag{9}$$

$$\tilde{\psi}(p) = \sqrt{\tilde{\rho}}\exp\left(i\tilde{\phi}\right)\,, \tag{10}$$

where $\psi, \tilde{\psi} \in \mathbb{C}$ are single valued functions of x and p respectively. To define a stream, we specify a single valued line in either position or momentum space where at each point the amplitude defines the density and the momentum or position is given by the derivative of the phase. For example, a stream s in real space is defined as:

$$\psi_s(x) = \sqrt{\rho}\exp\left(i\phi\right) \tag{11}$$

$$p_s(x) = \hbar\nabla_x\phi\,. \tag{12}$$

Likewise, a single value stream $\tilde{s}$ can be defined in momentum space as

$$\tilde{\psi}_s(p) = \sqrt{\tilde{\rho}}\exp\left(i\tilde{\phi}\right)\,, \tag{13}$$

$$x_s(p) = \hbar\nabla_p\tilde{\phi}\,. \tag{14}$$

We assume that these wavefunctions have been correctly normalized. To build up the equivalent of an

approximate phase space, we add up the contributions of different streams:

$$\psi = \frac{1}{\sqrt{N_s}} \sum_s^{N_s} \psi_s \,. \tag{15}$$

We will discuss below how this is an approximation for a phase space. It should be noted that formulating the wavefunction in this way makes phase space period in position position and momentum by construction. Because the momentum of our wavefunction is represented by oscillations on the grid the highest momentum that can be simulated before aliasing sets in is

$$p_{\max} = \hbar\pi/\Delta x \,, \tag{16}$$

where Δx is the grid cell spacing. Exceeding this maximum momentum will alias to the maximum negative momentum, and so on.

2. *Update*

The update rule for the Schrödinger-Poisson set of equations follows a scheme similar to the classical update outlined in Sec. II A. We start from the Schrödinger equation

$$i\hbar\dot{\psi} = H\psi = \left(\frac{p^2}{2m} + mV(x)\right)\psi \,, \tag{17}$$

where $p \equiv -i\hbar\nabla$. For slowly changing Hamiltonians, the wavefunction update between time t_0 and t_1 can be approximated as follows [25]:

$$\psi_{t1} = \exp\left(\int_{t0}^{t1} \frac{-iH}{\hbar} dt'\right)\psi_{t0} \equiv U(t_1, t_0)\psi_{t0} \,, \tag{18}$$

where $U(T, t)$ is the unitary operator which takes the wave function at time t to the wavefunction at time T. Note that, "slowly changing" in this context means the time step is chosen such that [17]

$$\frac{H\,\Delta t}{\hbar} \ll 1 \,. \tag{19}$$

Discretizing this equation we find the wave function after T time steps of length dt is given

$$\psi_T = \exp\left(\frac{-i\,H}{\hbar}\Delta t\right)\psi_{T-1} \,, \tag{20}$$

which will be accurate when $\frac{H}{\hbar}dt \ll 1$. We also notice that the Hamiltonian is separable into terms which depend only on the momentum or only on position. We can therefore rewrite the Hamiltonian as potential and kinetic terms

$$H = T(p) + V(x) \,. \tag{21}$$

This also implies that the operator $U(T, t)$ can also be written as a product of two terms,

$$U(\Delta t) = \exp\left(\frac{i\,\Delta t\,p^2}{2m\hbar}\right)\exp\left(\frac{-i\,\Delta t\,m\,V}{\hbar}\right) \tag{22}$$

$$= U_T(\Delta t)U_V(\Delta t) \,. \tag{23}$$

Notice that U_T is diagonal in the momentum basis and that U_V is diagonal in the position basis. Also recall that position and momentum are related by Fourier transform and so the momentum density of our wavefunction is represented by the k-space wavefunction scaled appropriately. This means that the update can be separated into two parts - the first changes the phase of the configuration space wavefunction, and the second changes the phase of the momentum space wavefunction. The update and density deposit rules are described in Table I. To compute the potential, we follow the same procedure as for the classical solver.

3. *Formal correspondence to and deviation from classical method*

Eqs. 12 and 14 imply that for a single stream, the derivative of the position space phase can give us the momentum of the stream at a given position, while the derivative of the momentum space phase can give us the position of the stream at a fixed momentum. For a single stream in phase space, at any phase space grid cell populated by a constituent packet of the stream, the position q and momentum p can be defined as

$$r \equiv \hbar\nabla_p\tilde{\phi} \,, \tag{24}$$

$$p = mv \equiv \hbar\nabla_x\phi \,. \tag{25}$$

Therefore, the derivative of our phases at that location in phase space gives us the position and momentum of that packet. Further, the amplitude of the wavefunction at that point gives the density at that (q, p) in phase space. Now recall that our update can be written as an update of the momentum space and position space phases respectively such that we can

rewrite our update rule as follows

$$\begin{aligned}\tilde{\phi}_{t+\Delta t} =& \tilde{\phi}_t + \frac{\Delta t\, p^2}{4m\hbar} \text{ (update position half step)}\\ &\text{(calculate V)}\\ \phi_{t+\Delta t} =& \phi_t + \frac{-\Delta t\, mV}{\hbar} \text{ (update momentum full step)}\\ \tilde{\phi}_{t+\Delta t} =& \tilde{\phi}_t + \frac{\Delta t\, p^2}{4m\hbar} \text{ (update position half step)}\end{aligned}$$

We can then use Eqs. 12 and 14 to re-cast the update rules as

$$\begin{aligned}r_{t+\Delta t} =& r_t + \frac{v\ \Delta t}{2} \text{ (update position half step)}\\ &\text{(calculate V)}\\ v_{t+\Delta t} =& v_t + a\ \Delta t \text{ (update momentum full step)}\\ r_{t+\Delta t} =& r_t + \frac{v\ \Delta t}{2} \text{ (update position half step)}\end{aligned}$$

where $a \equiv -\nabla_x V$. This set of update are exactly the same as those used for the classical solver. At face value, this would suggest that the classical solver and the Schrödinger-Poisson solver will agree with each other for any arbitrary setup. However, it should be noted that this exercise began with the assumption that we had an isolated single-valued stream in phase space. It is easy to define the derivative of the phase in either position space or momentum space for a one dimensional wave function provided there is only one stream. However, this is more challenging when we have multiple streams. Consider the simplest possible case of a system with two Gaussian streams with constant momenta $p_1 \equiv \hbar\nabla_x\phi_1$ and $p_2 \equiv \hbar\nabla_x\phi_2$ and identical position space densities $\rho_i/2$ where $\rho_i \sim \exp(-x^2)$. This wavefunction can be written as a super position as follows

$$\psi = \sqrt{\rho_i/2}\left(e^{p_1 xi/\hbar} + e^{p_2 xi/\hbar}\right). \tag{26}$$

Using the center of mass momentum $p_c = (p_1+p_2)/2$ and momentum difference $\Delta p = p_1 - p_2$, we can rewrite the above equation as

$$\psi = 2\sqrt{\rho_i/2}\cos(\Delta p x/2\hbar)\, e^{ip_c x/\hbar}. \tag{27}$$

Notice that the amplitude of the wavefunction oscillates as a function of the position, and depends on the momentum difference Δp. This stream interference present in the SP method has been noted in [11, 21, 24]. A higher separation in momentum leads to a more rapidly varying function in configuration space as noted in [21]. In fact the the amplitude of the wavefunction goes to 0 wherever the argument of the cosine term is equal to $(n+1)\pi/2$. It is straightforward to show that density is also spatially varying:

$$\rho = 2\rho_i \cos^2\left(\Delta p x/2\hbar\right). \tag{28}$$

However, we note that the average value of $\cos^2$ over a period is 1/2 and so the density is correct as long as we average over a distance $x_{av} = 2\pi\hbar/\Delta p$. This implies that higher the momentum separation of the streams, Δp, the smaller the length scale over which the density needs to be smoothed to reproduce the classical solution. Note that this means that the "classical limit", where the oscillation frequency becomes large, the oscillation present in the wavefunction remains order unity [11], however the fractional distance over which the average of the density approaches the correct value becomes small. Since our phase space is periodic in momentum space, there is an upper limit on the separation of the two streams along the momentum direction. This exercise, therefore, suggests that when the averaging length scale set by the momentum difference is smaller than the smallest dynamic length scale of the problem, x_D, the classical solution can be recovered. That is, our solution approaches the classical solution when

$$\frac{x_{av}}{x_D} = \frac{2\pi\hbar}{x_D\Delta p} \ll 1, \tag{29}$$

while our solution deviates strongly from the classical solution when the momentum separation between streams is too small (Fig 1), causing the oscillation term to be of order or greater than the smallest dynamic length scale. A similar argument as the one outlined above implies that for a one dimensional wavefunction representing two different streams in configuration space, the momentum space resolution has a bound:

$$\frac{p_{av}}{p_D} = \frac{2\pi\hbar}{p_D\Delta x} \ll 1. \tag{30}$$

It should be noted that it is also possible for a single stream, appropriately stretched and bent in phase space, to interfere with itself if it becomes double values as a function of p or x.

C. Von Neumann Poisson solver

As noted in Sec. II B, the Schrödinger-Poisson method of simulating classical systems is only valid for initial conditions which can be represented as a pure state. In this section, we present the Von Neumann solver relaxes the assumption contained the

Schrödinger-Poisson solver. Specifically, the solver follows the evolution of the density matrix of the system as opposed to a wavefunction; this allows for the correct evolution of mixed states, as well as pure states. Mixed states correspond to a classical statistical mixture or distribution of wavefunctions. A classical mixture of wavefunctions each exist in a separate Hilbert space and thus do not interfere with one another, opposed to quantum superpositions of different streams, where interference terms arise naturally.

The Von Neumann scheme increases the numerical scaling of the problem to $O(2n-D)$. However, there has been some interest in the solvers with this scaling [26], and in some cases where a continous velocity dispersion is necessary to recover the correct solution this solver may be preferable.

1. Initial conditions

The Von Neumann method requires the introduction of the density matrix P. This is represented as an $N \times N$ matrix in some basis. The diagonal of this matrix is the density in the chosen representation basis. As mentioned earlier, density matrices can represent a classical mixture of quantum states, unlike the wavefunction.

To populate the phase space, we can once again use the formalism of adding up multiple streams defined in position space in the following manner:

$$P(x,x') \equiv \frac{1}{N_s}\sum_{s}^{N_s} \psi_s(x)\psi_s^\dagger(x')\,, \tag{31}$$

where $\psi_s\psi_s^\dagger$ represents the outer product of the wavefunctions, and an individual stream is represented as before,

$$|\psi_s\rangle = \sqrt{\rho}\exp\left(i\phi\right)\,, \tag{32}$$

$$p = \hbar\nabla_x\phi\,. \tag{33}$$

Notice that P does not uniquely define a sum of streams, that is, there are infinite possible different summations which would give the same P. However, the evolution of P is unique. We index individual elements of the discretized matrix P with i,j such that $P \in \mathbb{C}^{N_s\times N_s}$ and $P_{i,j} \in \mathbb{C}$. Since the diagonal of P can be treated as a density in the position basis, $P_{i,i} \in \mathbb{R}$, i.e. the diagonal elements are real. The density in any basis is the diagonal of the density matrix represented in that basis.

2. Update

The evolution of the density matrix proceeds using the Von Neumann equation:

$$P_T = \frac{1}{N_s}\sum U(\Delta t)\psi_{T-1}\left(U(\Delta t)\psi_{T-1}\right)^\dagger \tag{34}$$

$$= U(\Delta t)P_{T-1}U^\dagger(\Delta t)\,. \tag{35}$$

Note that update operator U in the above equation is similar in form to the one in Eq. 18, and therefore also splits into independent updates of the position space phase and the momentum space phases of the matrix. The update and density deposit rules are described in Table I.

The potential is computed from the density described in Table I. Element-wise, the position and momentum update rules can be written as

$$\tilde{P}_{ij,t+\Delta t} = \tilde{P}_{ij,t}\exp\left[\frac{i\,\Delta t}{2\,m\,\hbar}(p_i^2 - p_j^2)\right]$$

$$P_{ij,t+\Delta t} = P_{ij,t}\exp\left[\frac{i\,\Delta t}{\hbar}(V_j - V_i)\right] \tag{36}$$

$$\tag{37}$$

where $\tilde{P}$ is the momentum space representation of the density matrix. This is computed by performing a Fourier transform on the axis labeled by i and an inverse Fourier transform on the axis labeled by j of the real space density matrix:

$$\begin{aligned}\tilde{P} &= \langle p_i|\,P\,|p_j\rangle \\ &= \int\int dx_i dx_j\,\langle p_i|x_i\rangle\,\langle x_i|\,P\,|x_j\rangle\,\langle x_j|p_j\rangle \\ &= \int\int dx_i dx_j e^{\frac{i}{\hbar}(p_j x_j - p_i x_i)}P_{x_i,x_j} \\ &= F_1^{-1}(F_0(P))\,,\end{aligned} \tag{38}$$

where F_0, F_1 represent the Fourier transform along axis 0 (horizontal) and axis 1 (vertical) repsectively.

3. Formal correspondence to and deviation from classical method

For a single stream, the correspondence of the Von Neumann method with the classical solution can be shown using the same method as presented in Sec. II B 3 - the only difference being that we start with the density matrix instead of the wavefunction. This result is expected since the single-stream scenario represents the equivalent of a pure state in

our formalism, and the Schrödinger and the Von Neumann approach are formally equivalent for pure states.

The two-stream scenario, on the other hand, as represented in the density matrix setup is a mixed state, and the Von Neumann and Schrdinger approaches produce different results. To show this, we once again consider two streams with momenta $p_1 \equiv \hbar\nabla_x\phi_1$ and $p_2 \equiv \hbar\nabla_x\phi_2$ and identical position space densities $\rho_0/2$. We write our density matrix as

$$P_{i,j} = \frac{\rho_0}{2}\left[\exp\left(\frac{i\,p_1}{\hbar}\,(x_i - x_j)\right) + \exp\left(\frac{i\,p_2}{\hbar}\,(x_i - x_j)\right)\right]. \tag{39}$$

The density field is therefore given by

$$\rho = \mathrm{diag}(P) = \frac{\rho_0}{2}\left(e^0 + e^0\right) = \rho_0\,. \tag{40}$$

The density field has the correct value (Fig 1). The oscillations that were present in the density field in the Schrödinger solver for two stream are thus eliminated in the Von Neumann method. This implies that different streams no longer quantum mechanically interfere with each another. However, streams can still interfere with themselves when they become highly distorted in phase space.

D. Multiple Hilbert spaces

As we saw in Sec. II B 3, interference between different streams leads to the breakdown of the correspondence between the classical solution and the Schrödinger-Poisson solution. Since interference terms only arise for wavefunctions defined on the same Hilbert space, this problem can be mitigated by defining each stream in its own Hilbert space as in [13]. The individual Hilbert spaces are then evolved in the joint potential. Since the underlying variables of this method are 1-dimensional wavefunctions, rather than the full density matrix, this method has lower computational cost than the Von Neumann method - the Von Neumann method scales as $\mathcal{O}(N^2)$, while the Schrödinger method scales as $\mathcal{O}(N)$. Therefore evolving wavefunctions in multiple Hilbert spaces scales as $\mathcal{O}(n_s N)$, where n_s is the number of streams, and N is the grid size. Since in most cases $n_s \lesssim \mathcal{O}(10)$, while $N \gg 1$, this represents a large speedup over the Von Neumann method.

1. *Initial conditions*

The object of interest in this method is a vector of wavefunctions Ψ where

$$\Psi_i = \frac{1}{\sqrt{N_s}}\psi_i\,. \tag{41}$$

Therefore the i-th element in the vector represents the i-th stream, with each stream defined the same way as before.

2. *Update*

Each individual stream, i, is updated using the same procedure as outlined in Sec. II B 2. The only difference is that the density that enters the Poisson solver is the one described in Table I.

3. *Formal correspondence to and deviation from classical method*

Again the same definitions of p and r will reproduce the classical update rule as before. Returning to the two stream test problem. We find that our vector can be written with two components as

$$\Psi_0 = \sqrt{\frac{\rho_0}{2}}e^{ip_0 x/\hbar}\,,$$
$$\Psi_1 = \sqrt{\frac{\rho_0}{2}}e^{ip_1 x/\hbar}\,. \tag{42}$$

Eq. 41 implies that the density for this system is given by

$$\rho = |\Psi_0|^2 + |\Psi_1|^2 \tag{43}$$
$$= \frac{\rho_0 + \rho_0}{2} = \rho_0\,. \tag{44}$$

Therefore, this method recovers the correct density (Fig 1), that is, the density is constant in space, without the interference terms which appeared Sec. II B 3.

III. QUANTUM PHASE SPACE REPRESENTATION

Phase space representations of quantum states typically have properties that deviate from those of classical phase space representations. Wigner and

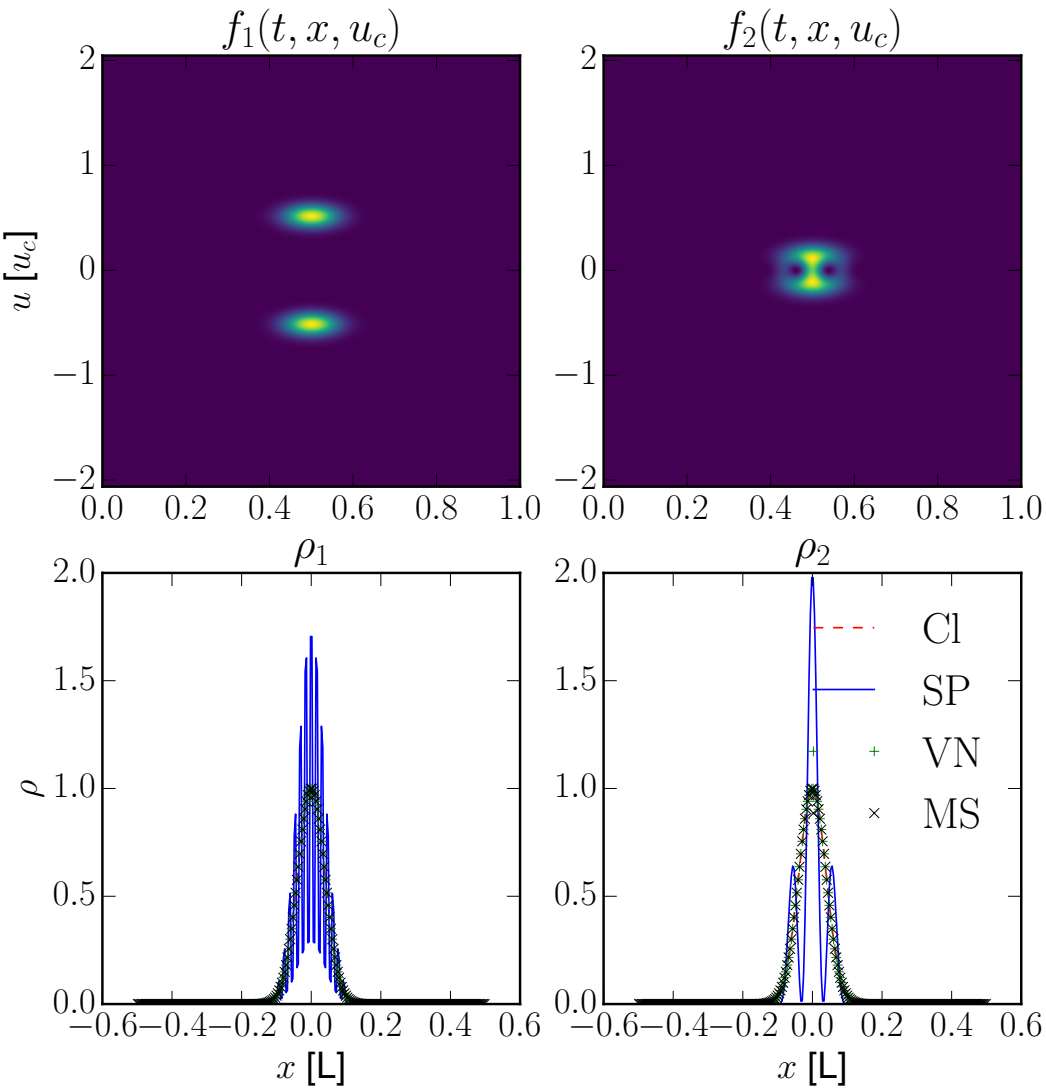

FIG. 1. Plot of the SP quantum phase space representation and spatial density of two Gaussian streams. The left column shows the results for well separated streams, the right column shows poorly separated streams. The wavelength of the oscillation in the SP spatial density decreases as the stream velocity separation increases. The oscillation structure can also be seen in the interference fringes between the stream representations in phase space (top right). All other methods lack the oscillation and match the classical density profile.

Husimi distributions have both been used [7, 11, 15–18, 23, 24, 27]. However, Wigner distributions are only everywhere positive when the quantum state is a super position of gaussians and the Husimi distribution does not recover the correct moments of the given distribution [25]. Here we use the Husimi distribution, which has the advantage of being everywhere positive, as an approximation of classical phase space. When interpretation the Husimi distribution as an approximation of the classical phase space it is important to recall that structures in phase space below the characteristic area of the smoothing kernel cannot be resolved.

The Husimi function represents a mapping from

a state to phase space. The phase space itself is composed of basis states for a given position (q) and momentum (p) in phase space given as follows [25] (in the position basis of our wavefunction)

$$\langle x|q,p\rangle \equiv (2\pi s^2)^{-1/4} e^{-(x-q)^2/4s^2} e^{ipx/\hbar_1} \tag{45}$$

in which $s \in \mathbb{R}$ is a free parameter. These states are obviously not orthogonal but can be made to form a resolution to the identity as follows

$$(2\pi\hbar)^{-1} \int |p,q\rangle \langle p,q| \, dpdq = I \tag{46}$$

In general the phase space distribution ($f_H(q,p)$) can be obtained by taking the modulus squared of the wavefunction evaluated in the (q,p) basis states. Note however that,

$$|\psi(q)|^2 \neq \int_{\text{All}} f_H(q,p)dp \tag{47}$$

$$|\psi(p)|^2 \neq \int_{\text{All}} f_H(q,p)dq \tag{48}$$

Finding the probability distribution for each quantum solver then simply involves taking an inner product of the basis states with the wavefunctions or density matrices, described in Table II.

IV. TEST CASES

In this section we present the results of simulations of various test cases using the different methods outlined in the previous section. For every test problem, we use the classical solver as a benchmark for the accuracy of the other solvers.

A. Cold stream distributions

The systems here represented correspond to classical plasmas composed of a large number of particles with common mass and charge. The system can be described by a continuous phase space obeying the Vlasov-Poisson equations in which the potential is sourced by the charge density of the particles. When the relevant physics involves a small number of cold streams, well resolved in phase space, all the quantum solvers are capable of reproducing the classical result. We demonstrate this correspondance by simulating two stream instability and sine wave collapse.

1. *Two stream instability*

Our first test problem is 1D two stream instability, a classic instability relevant in the evolution of cold plasmas [28, 29]. This problem demonstrates the ability of all of our solvers to accurately model multiple cold streams well resolved in phase space and recover the expected instability. Two streams at different velocities are given an initial perturbation. We set up the system with the two cold streams spaced apart in phase space such that their velocity separation is less than twice the critical velocity u_0 (See Appendix for the definition of u_0). The initial perturbation will then grow exponentially for a time following these initial conditions [12, 13, 28].

We initialize streams with the dimensionless velocity $u_s \approx \pm.8$ (See Appendix for the definition of u_s), and introduce a sinusoidal perturbation to the stream velocities with perturbation wavelength equal to the size of the box and amplitude $\delta u = .05u_0$. The amplitude of the perturbation over time can be measured (when the perturbation is approximately linear) by looking at the maximum value of electric field. For these simulations we use $N = 256$ grid cells, $n = 2^{16}$ particles in the classical solver, $\hbar = 1x10^{-6}$, and the Poisson constants for the quantum and classical solvers are $C_Q = -6x10^{-6}$ and $C_{cl} = -1$ respectively.

It has been previously demonstrated that classical two stream instability can be reproduced using quantum methods [12, 13, 24]. We find that all four methods produce the same perturbation growth, i.e. all the quantum solvers agree with the classical solution, as well as with each other. This is shown in Fig.2, where we find that the electric field from all the implementations broadly agree. There are some quantitative difference between the Schrödinger solver and the other solvers at early times, but these disappear with time. We also plot the phase space from each simulation in Fig. 3, which corroborates the idea that all the solvers produce a similar time evolution, in good agreement with our expectations. All the quantum solvers, including the Schrödinger Poisson method, are expected to perform well for this test because the separation of the streams is well resolved in phase space. This means that any interference terms in the SP solver to have a vanishing effect on the large scale physics.

We note that [12, 13] presented a detailed analysis of the quantum and classical correspondence for two stream instability by scanning over two dimensionless parameters. The parts of parameter space which deviated strongly from the classical results are

	Schrödinger	multiple Hilbert spaces	Von Neumann
$f_H(q,p)$	$(2\pi\hbar)^{-1}\left\|\langle q,p\|\psi\rangle\right\|^2$	$(2\pi\hbar)^{-1}\langle q,p\|P\|q,p\rangle$	$(2\pi\hbar)^{-1}\sum_i^{n_s}\left\|\langle q,p\|\Psi_i\rangle\right\|^2$

TABLE II. Shown for each quantum solver is the equation for the Husimi phase space.

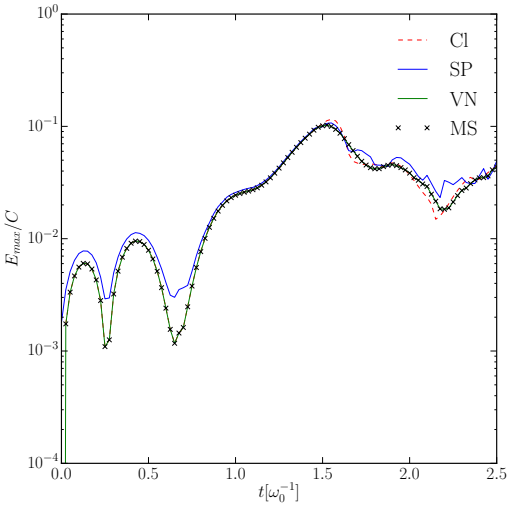

FIG. 2. Plotted is the maximum value of the E field as a function of time for two stream instability simulations for each solver. All four solvers agree quite well even at relatively late times. At early times, when the perturbation is small, you can see that interference terms wash our the smallest scale structure in the SP case, this does not however, prevent later agreement.

exactly those regions which resulted in the streams being more poorly resolved in phase space compared to the velocity resolution of the simulation. This is in good agreement with the results derived in Sec. II B 3.

2. *Sine wave collapse*

We now consider the gravitational collapse of a sine wave perturbation, a standard phenomena in self gravitating plasmas. The perturbation will grow exponentially resulting in density shell crossings and a characteristic spiral structure in phase space [30]. There has been much discussion of the behavior of quantum solvers during shell crossing [15, 16, 18]. When this occurs the density and wavefunction go to zero. Formally, this means that the phase of the wavefunction at these points is not well defined. Therefore, it is useful to demonstrate the ability of our solvers to reproduce the classical results in systems where shell crossing occurs.

In the one dimensional case we initialize a cold stream with a sinusoidal velocity perturbation with wavelength equal to the size of the box and amplitude $\delta u = .05u_0$. For these simulations we use $N = 512$ grid cells, $n = 2^{12}$ particles in the classical solver, $\tilde{\hbar} = 7x10^{-7}$, and the Poisson constants for the quantum and classical solvers are $C_Q = 2x10^{-6}$ and $C_{cl} = 1$ respectively. We track the phase space of each solver in Fig. 4.

In the two dimensional case we initialize a cold stream with a sinusoidal velocity perturbation in x with wavelength equal to $L/3$ and a velocity perturbation in y equal to $L/2$ both with amplitude $\delta u = .1u_0$. For these simulations we use $N = 64$ grid cells, $n = 2^{23}$ particles in the classical solver, $\tilde{\hbar} = 7x10^{-7}$, and the Poisson constants for the quantum and classical solvers are $C_Q = 2x10^{-6}$ and $C_{cl} = 1$ respectively. We track the spatial density of each solver in Fig. 5.

As previously demonstrated in [15, 17] the quantum solvers are capable of reproducing the expected results in both one and two dimensions. The phase space in Fig. 4 shows good agreement between all methods. The small scale structure at the center of the spiral at late times is below the Husimi length scale and as expected is washed out, however, the large scale spiral structure is reproduced.

B. Warm stream distributions

The first place that the SP solver begins to fail is for conditions which contain streams that are poorly resolved in phase space. Any conditions with a continuous non zero velocity dispersion would be considered warm conditions for which stream resolution is not possible. These cases are also of interest to astrophysics and so we demonstrate the ability of the multi stream and VN solvers to reproduce the classical results for Landau damping, bump on tail instability, and Jean's instability.

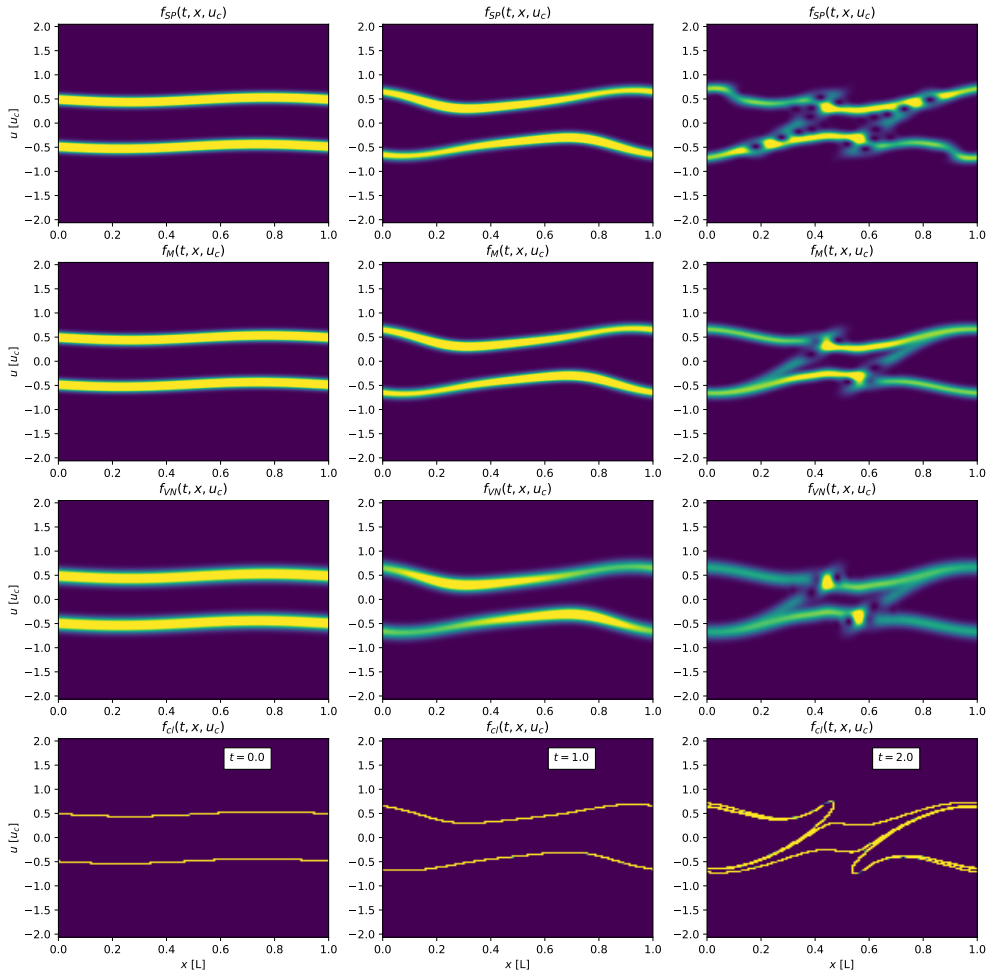

FIG. 3. The phase space for two stream instability. Each row represent a different solver and each column a time. All four solvers show the same evolution. The right image in the top row shows interference present in the phase space due to streams overlapping in both position and velocity space. The right images in the middle two rows show interference due to streams interfering with themselves in velocity space for the VN and MS methods.

1. *Landau damping*

We turn now to the test problem is Landau damping. This effect dampens plasma oscillations by allowing lower energy particles to "surf" perturbations which transfers energy from the perturbation to the particles [29]. We expect initial perturbation amplitudes to exponentially dampen [22, 26, 29]. This test problem will demonstrate the ability of our quantum solvers to represent the interaction of many streams in a warm distribution as well as track the expected decay of perturbations up to and beyond where the classical solver can produce.

Landau damping is driven by the derivative of the dispersion relation [29]. Therefore, the correct initial conditions is a warm stream with a continuous

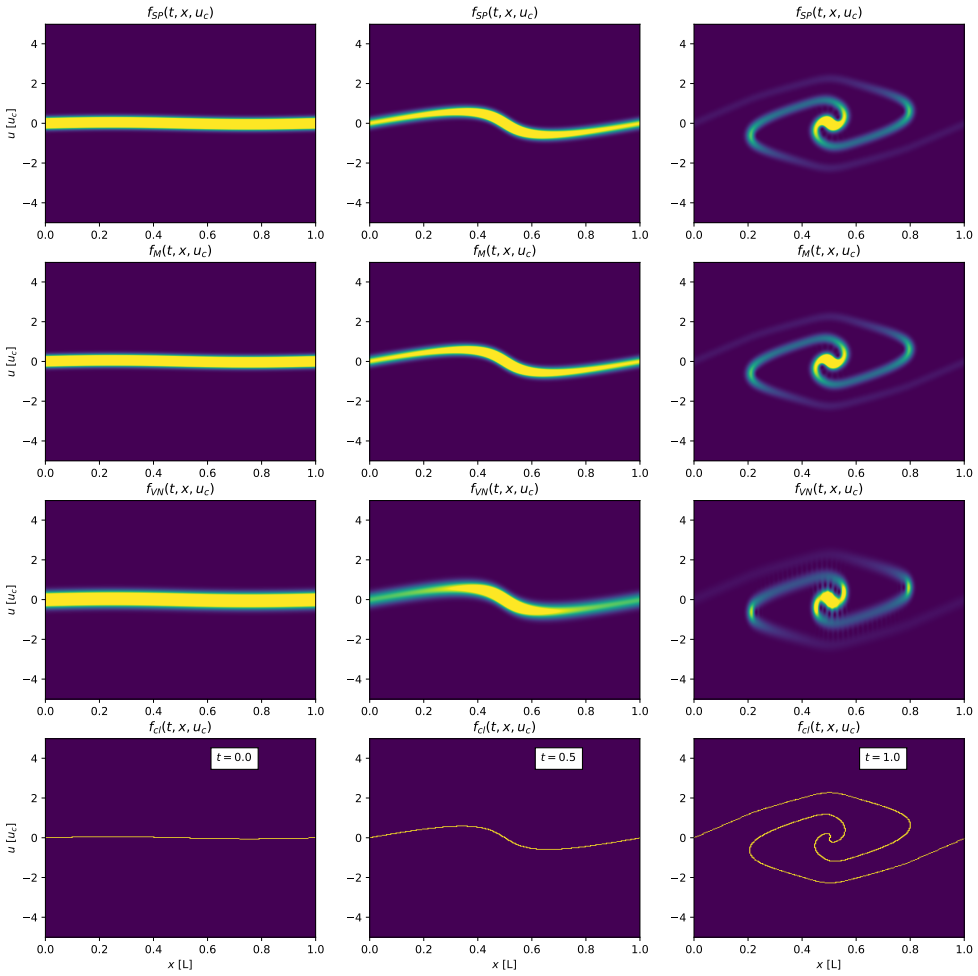

FIG. 4. The phase space for sine wave collapse. Each row represent a different solver and each column a time. All four solvers show the same evolution.

velocity dispersion as opposed to a small number of interacting cold streams. The initial conditions are a warm stream with Gaussian velocity dispersion with mean $v_{offset} = 0$ and standard deviation $v_{th} = .49$. All streams are initialized with velocity perturbation $\delta u = .05u_0$. For these simulations we use $N = 256$ grid cells, $n = 2^{16}$ particles in the classical solver, $\hbar = 1x10^{-6}$, $N_s = 200$ streams, and the Poisson constants for the quantum and classical solvers are $C_Q = -2x10^{-6}$ and $C_{cl} = -1$ respectively. We track the amplitude of the density by following the maximum of the electric field over time in Fig. 6.

The multi stream and VN solvers reproduce the correct results. The electric field clearly for these methods clearly shows the expected exponential decay. The success of the multi stream method was predicted in [13], although it was not demonstrated. The SP solver is unable to reproduce the correct results because the streams are not well resolved in phase space and thus the aphysical interference

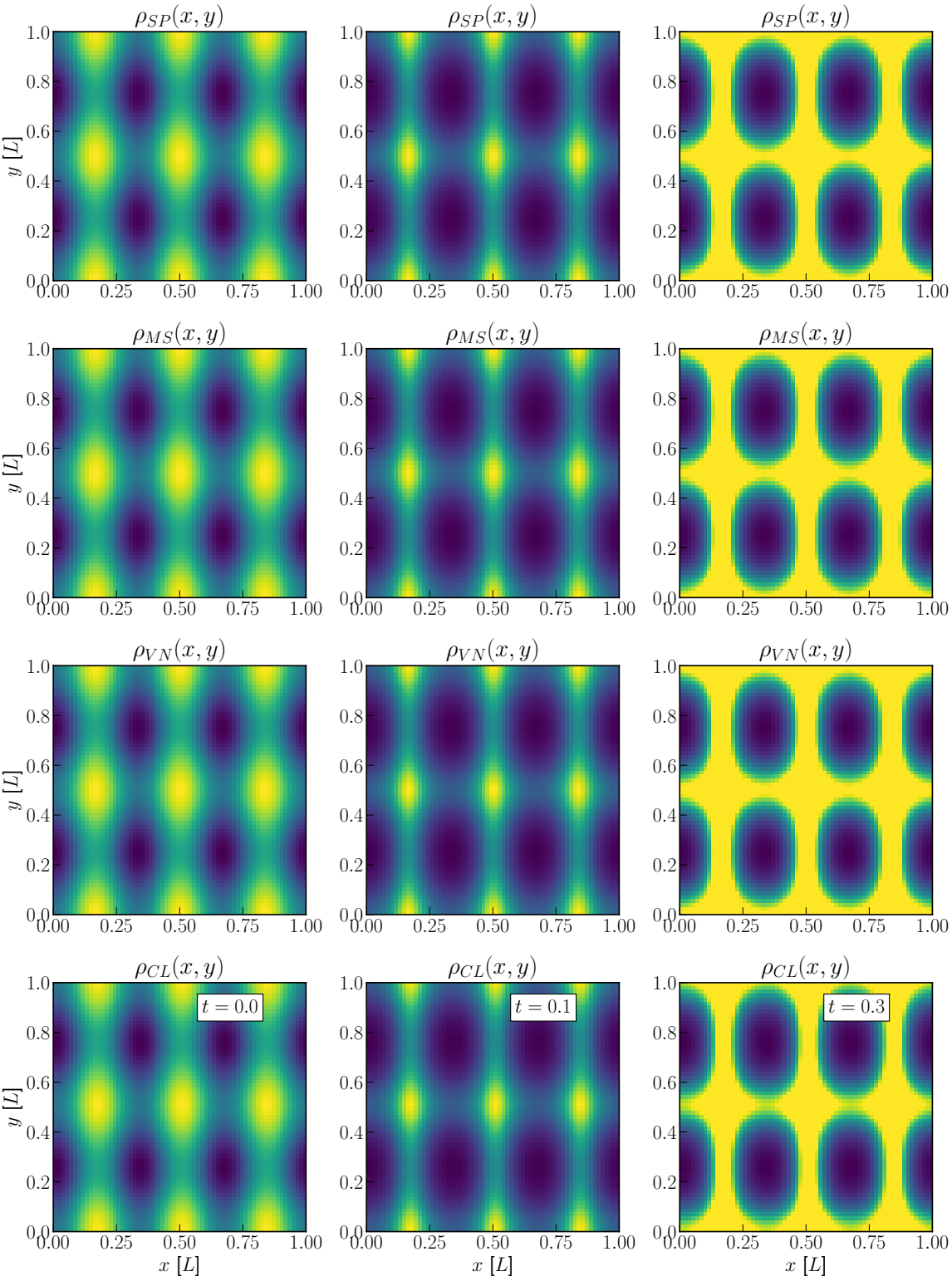

FIG. 5. The density for two dimensional sine wave collapse. Each row represents a different solver and each column a time. All four solvers show the same evolution.

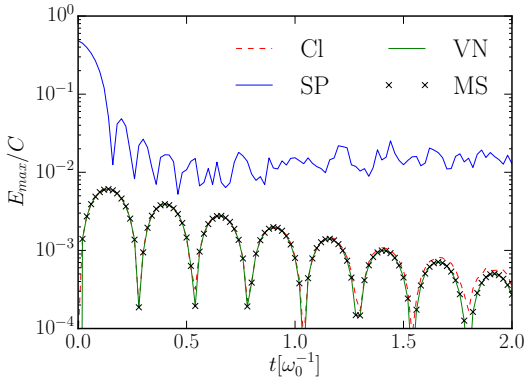

FIG. 6. Plotted is the maximum value of the E field as a function of time for Landau damping simulations for each solver. The SP solver fails to reproduce the correct results as the interference terms between the many streams in the system dominate the evolution. The VN, MS, and classical solvers are in good agreement. At late times spurious structures in the classical solver cause it to deviate from the expected exponential decay.

terms dominate the simulation. It has been shown in [22] that an ensembled average of SP solver simulations can produce Landau damping. No such averaging is necessary using the multi stream and VN methods. Additionally, a direct integration of the Wigner function on phase space has been shown in [23] to reproduce Landau damping. However, as we have demonstrated here it is not necessary to represent the entire phase space.

The multiple stream interference prevents a simple simulation of Landau damping for the SP solver. If however, we try and represent the same problem but with a decreasing number of streams we can see how the interference terms affect the evolution by plotting the potential for $N_s = 7$ and $N_s = 33$ in Fig. 8 and Fig. 7 respectively. The SP is able to track the solution of the other solvers better when the number of streams is decreased, however as the number increases the interference terms begin to dominate.

Also plotted in Fig. 7 and Fig. 8 is the quantum potential term for the SP solver given as [25]

$$V_{QM} = -\frac{\hbar^2}{2m}\frac{\nabla^2|\psi|}{|\psi|} \tag{49}$$

The existence of the quantum potential term when developing the SP system from the Madelung representation is frequently mentioned [11, 13, 15, 16, 18]. However, in the simulations presented in this section, the quantum potential remains no larger than $\sim 10^-4$ times smaller than the classical potential and has a vanishingly small effect on the dynamics of the system. Despite this, the SP solver still begins to diverge from the correct evolution in 7 due to the inability to accurately represent the density. It should be noted that investigating the quantum pressure term is not sufficient to describe the SP deviation from classical solutions.

2. *Bump on tail instability*

Bump on tail instability results in plasmas in which a small over-density at a velocity separated from the background plasma velocity is unstable to perturbations. The importance of bump on tail instability to plasmas dynamics is discussed in [31]. Here we use the instability to again demonstrate the ability of our quantum solvers to produce accurate results for warm stream conditions by correctly tracking velocity density and phase space.

Bump on tail instability again involves a continuous velocity dispersion. We start with an initial background distribution with mean velocity $v_{offset} = 0$ and thermal velocity $v_{th} = .07$. A bump is created with mass $M_{bump}/M_{background} = .1$ and velocity offset $v_{bump} = .7$ and the same velocity dispersion as the background. All streams are initialized with velocity perturbation $\delta u = .05u_0$. For these simulations we use $N = 256$ grid cells, $n = 2^{16}$ particles in the classical solver, $\tilde{\hbar} = 1x10^{-6}$, $N_s = 200$ streams, and the Poisson constants for the quantum and classical solvers are $C_Q = -6x10^{-6}$ and $C_{cl} = -1$ respectively. We plot both the phase space in Fig. 9 and the velocity density in Fig. 10 over time. As expected the multi stream and VN solvers reproduce the classical results. We see excellent agreement both in the evolution of the phase space and the velocity density.

3. *Jean's instability*

For warm distributions subject to their own gravity the Jean's length determines which modes will be stable or unstable. Perturbations with length greater than the Jean's length will be undergo exponential growth while perturbations with length less than the Jean's length will undergo exponential decay [26]. This test problem will demonstrate the ability of our quantum solvers to reproduce the correct evolution of the power spectrum at early times for warm initial conditions.

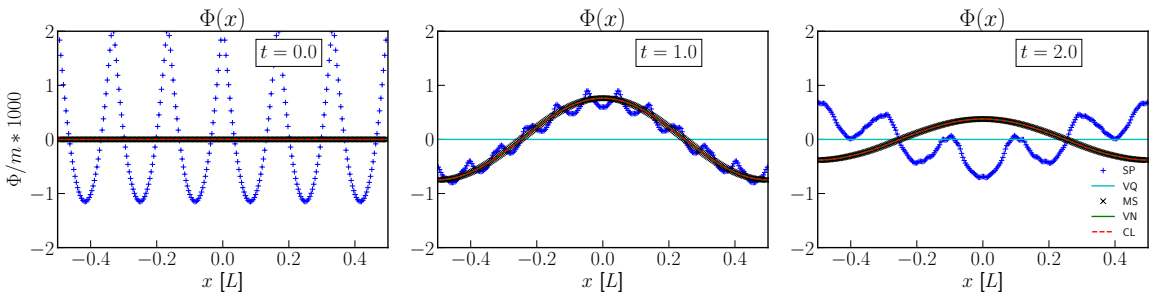

FIG. 7. Plotted is the potential for each solver at three different times for a Landau damping simulation using $N_s 33$. Also plotted is the quantum potential. The relatively large number of streams produces interference terms in the SP solver that

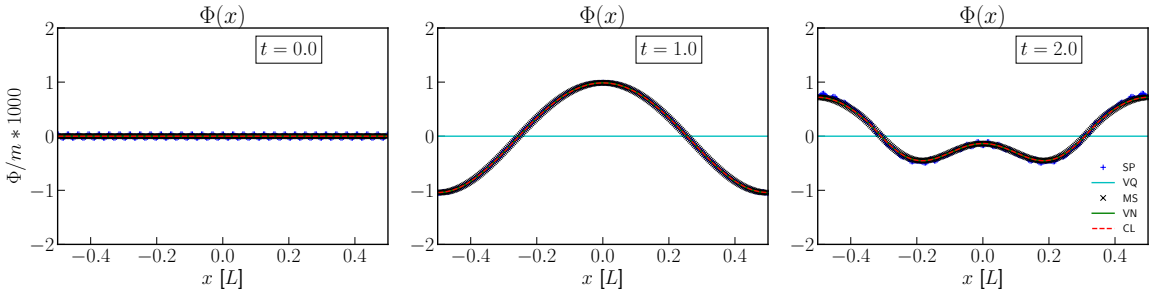

FIG. 8. Plotted is the potential for each solver at three different times for a Landau damping simulation using $N_s = 7$. The few streams can be accurately represented by the all solvers.

We start with an initial velocity distribution with $v_{th} = .15$. We then produce a flat intial power spectrum for $k \in [0, 32\pi/L]$ by adding spatial perturbations with wavelengths $\lambda = [L/1, L/2 \ldots, L/16]$ of initial size $\delta_x = .05$. For these simulations we use $N = 512$ grid cells, $n = 2^{16}$ particles in the classical solver, $\tilde{\hbar} = 1 \times 10^{-7}$, $N_s = 240$ streams, and the Poisson constants for the quantum and classical solvers are $C_Q = 2x10^{-6}$ and $C_{cl} = 1$ respectively. We plot the power spectrum over time in Fig. 11. We find the multi stream and VN solvers reproduce the expected results.

V. DISCUSSION

A. Interference

The most obvious problem with quantum solvers is interference between streams that are poorly resolved in phase space. The interference term comes from the inability of a single valued function of momentum or position to represent a multivalued phase space, i.e. multiple streams. This is most problematic for the Shroedinger Poisson solver with only a single wavefunction. The interference between overlapping streams can be overcome by separating the Hilbert spaces of the streams by either putting them into a classical mixture as in the Von Neumann solver or by separately evolving each stream in a shared potential. However, it should be noted that this does not prevent streams from interfering with themselves if a single stream becomes multivalued in either position or momentum.

Interference can have a large effect on the ability of solvers to approximate the classical solution. If the interference occurs over length or momentum scales that are relevant to the evolution of the system the solver may deviate strongly from the classical solution. It should also be noted that interference can prevent a solver from being accurate even where the quantum pressure term is vanishingly small. Therefore, understanding the SP system as differing from classical fluid dynamics by this term alone is insuf-

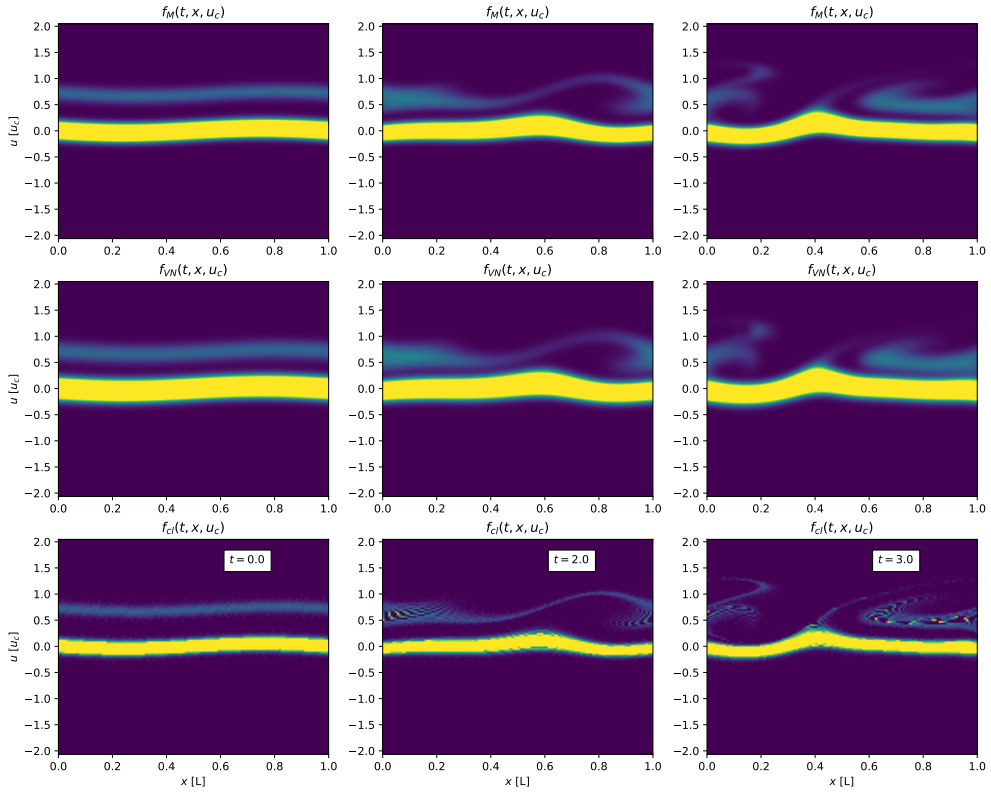

FIG. 9. The phase space for bump on tail instability. Each row represent a different solver and each column a time. All three solvers show the same evolution.

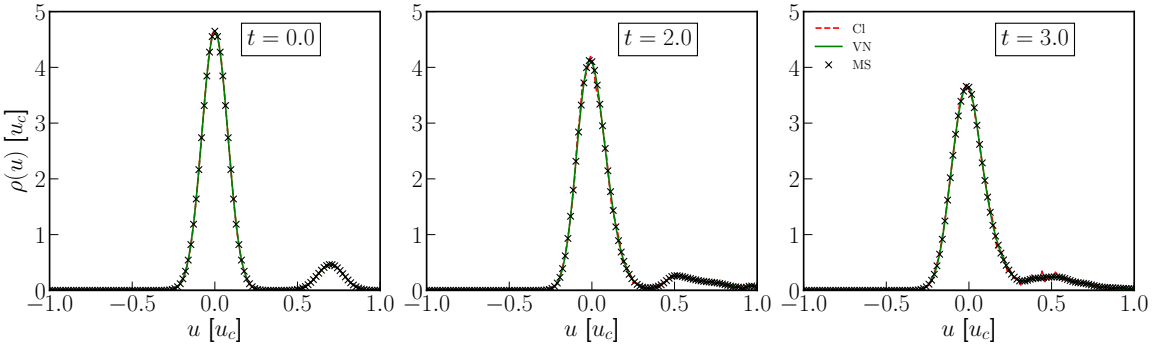

FIG. 10. The velocity density over time for each solver for bump on tail instability. All three solvers show the same evolution.

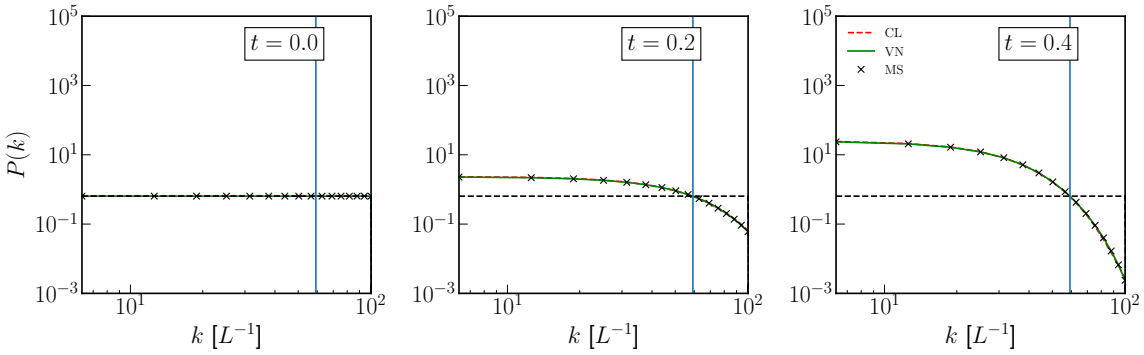

FIG. 11. The power spectrum overtime for Jean's instability for each solver. The vertical blue line represents the Jean's scale for this simulation, modes to the left should grow and modes to the right should be damped. The horizontal black dotted line shows the initial power spectrum. All three solvers show the same expected growth of modes below the Jean's scale and damping of modes above the scale.

ficient to produce the correct classical approximations.

Recall that the relevant quantity governing the interference is proportional to $\hbar$. This alludes to the physical constant but in these simulations is just a free parameter governing the relationship between the numerical representations of position and momentum. Therefore, we can arbitrarily decrease the interference between streams by simply lowering the value of $\hbar$. This of course incurs another problem discussed in the next section.

B. Fixed maxima and aliasing

The momentum and position representations of the wavefunction encode information about density in phase space by using derivatives of the complex angle in the wavefunction. The maximum wavenumber that can be accommodated by a finite grid of size N and physical length L is

$$k_{\max} = N\pi/L\,. \tag{50}$$

Momentum and wavenumber are related by $p = \hbar k$, implying that the maximum physical momentum that can be represented in the system is fixed by the starting grid size and choice of $\hbar$ and L. Consequently, while a wider range of physical momenta can be achieved by increasing $\hbar$, this also increases the influence of interference terms. This means the classical limit is only achieved by making N large and not by varying the value of $\hbar$. The fact that position and momentum are related by the Fourier transform on a finite grid means that the phase space is periodic in both momentum and position space. Therefore, while periodic positions are generally not problematic, the maximum momentum present in the simulation should be checked against the maximum allowed moment to prevent the formation of spurious structures as in Fig. 12.

C. The classical limit

Generally when we want to the limit in which a quantum system becomes classical we take the limit $\hbar \lim 0$. However, it is not immediately clear what this limit is taken with respect to. It becomes increasingly confusing when $\hbar$ represents not a physical constant but a simulation parameter, as when using quantum solvers for classical problems.

It is clear from the Madelung formalism, discussed in other works [11, 13, 15, 16, 18], that $\hbar$ should be sufficiently small such that the quantum potential term is small compared to the classical potential. i.e. $\tilde{\hbar} = \hbar/m$ must be chosen such that

$$\tilde{\hbar} \ll \frac{|\psi|\ V_{cl}}{\nabla^2|\psi|} \tag{51}$$

However, we have shown that this is insufficient to assure that the classical solution is obtained. We must also consider the interference terms in the representation of the density. Let us again consider two streams separated by Δp in phase space. As we take $\hbar \lim 0$ the density will never approach the classical density. Instead the frequency of the oscillation will

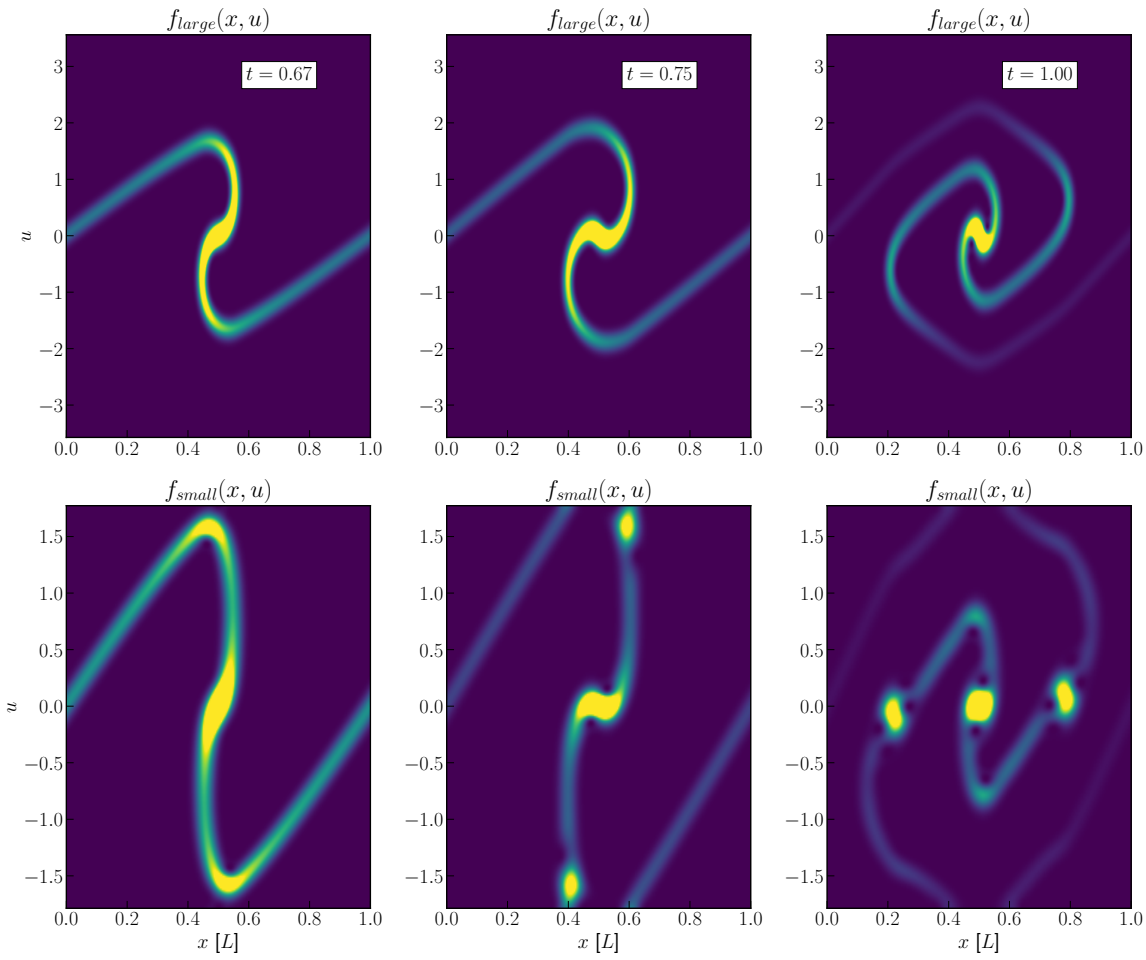

FIG. 12. Shown is the phase space for sine wave collapse with $\tilde{\hbar} = 5x10^{-7}$ with $N = 512$ and $N = 256$ grid cells for the top and bottom rows respectively. Between $t = .67$ and $t = .75$ the simulation attempts to represent velocities beyond the maximum allowed velocity in the smaller simulation. The bottom row shows how this creates spurious over densities in phase space that persists in the simulation.

increase, meaning a smaller and smaller spatial average will be needed to approach the classical solution. The distance over which it is necessary to average to achieve the classical density must be small compared to the dynamical length scale of the system x_D. By taking the necessary spatial average to be the order of the wavelength of the interference we can say that

$$\hbar \ll \Delta p\ x_D \tag{52}$$

must also be satisfied. Qualitatively, this can be thought of as an area in phase space. Multiple streams sharing a phase space region on the order of $\hbar$ will begin to deviate from the classical solution. However, the appropriate orientation of this phase space area depends on the relevant x_D at a given point and so this interpretation of $\hbar$ should be used conservatively.

VI. CONCLUSIONS

We have demonstrated that quantum solvers can be used to approximate the classical evolution of a number of plasma and gravitational systems. Single wavefunction quantum solvers, such as our Schrödinger Poisson solver, can simulate initial conditions in which there are few well resolved streams. Furthermore, we have shown that introducing additional wavefunctions, as in our multiple Hilbert

solver, we can extend the region of validity of quantum solvers to include warm initial conditions where streams may be in a velocity dispersion or very close in phase space. We have also introduced a new extension using the density matrix formalism and Von Neumann equation. This solver is somewhat analogous to phase space solvers in that it is a $2n$ dimensional solver, where n is the number of dimensions. We have demonstrated that this solver can also be used to simulate warm distributions.

The limit in which this classical approximation are valid is both where the quantum potential is small compared to the classical potential and where the dynamical length scale is large compared to the interference terms in the quantum solver density representations. Likewise, parameters must be chosen such that the simulation does not attempt to exceed the maximum velocity allowed by the solver. However, if these conditions are met it is possible to simulate a wide variety of classical phenomena.

Developing a method that would adaptively resize or change simulation parameters may provide a more robust solver. Given the potential usefulness of representing $2n$ degrees of freedom in an n dimensional wavefunction, it would be interesting to produce solvers that more carefully adhere to classical solutions. More work comparing the accuracy of the Von Neumann solver to full phase space solvers was not included in this work but would further explore the utility of this extension.

Appendix: Units

In this Appendix, we discuss how we create a set of dimensionless units for length, velocity, and time, which define our code units. All positions and lengths are measured in units of the simulation box, L, such that $0 \leq x_s \leq 1$. For certain test problems, we also adopt $-0.5 \leq x_s \leq 0.5$. All perturbation length scales λ for the plasma problems are defined in these length units. Next, we cast Poisson's equation as

$$\nabla^2 \phi = C\rho \,, \tag{A.1}$$

noting that C can be greater or less than 0. $C > 0$ represents attractive forces, while $C < 0$ represents repulsive forces. In the eletromagnetic systems, we define a frequency in the following manner:

$$\omega_0 = \sqrt{\frac{-C}{2}} \,. \tag{A.2}$$

We also define a time and velocity unit as

$$t_0 = \frac{2\pi}{\omega_0} \,, \tag{A.3}$$

$$u_0 = \frac{\lambda \omega_0}{\sqrt{2}\pi} \,. \tag{A.4}$$

Note that the unit for velocity is motivated by the critical velocity in two stream instability. We normalize the total mass in the system to unity, i.e. $M_{tot} \equiv 1$. For the plasma problems, we can also define a unit of electric field.

$$E_0 = \frac{C}{M_{tot}} \,. \tag{A.5}$$

Using these definitions we can define the following dimensionless simulation units for length, mass, time, velocity, and electric field respectively

$$x_s = \frac{x}{L} \in [0,1] \ \textit{or} \ [-.5,.5] \,, \tag{A.6}$$

$$m_s = \frac{m}{M_{tot}} \in [0,1] \,, \tag{A.7}$$

$$t_s = \frac{t\sqrt{-C}}{2\pi\sqrt{2}} = \frac{t}{t_0} \,, \tag{A.8}$$

$$u_s = \frac{2\pi u}{\lambda\sqrt{-C}} = \frac{u}{u_0} \,. \tag{A.9}$$

For our non-classical solvers we also need to choose a value for $\tilde{\hbar} \equiv \hbar/m_{\text{part}}$ which describes the relationship between position and momentum in these solvers.

Appendix: Von Neumann generalization to 3D

In this Appendix we discuss how to generalize the Von Neumann solver to higher dimensions by example with the three dimensional case. The fundamental object, the density matrix, P, is a $2n$ dimensional object still given by the sum of the outer product of stream wavefunctions, which can be written element-wise as:

$$P_{iljmkn} \equiv \frac{1}{N_s} \sum_{s}^{N_s} \psi_{ijk,s} \psi^*_{lmn,s} \tag{A.1}$$

$\tilde{P}$ can then be calculated using a series of Fourier transforms. Here we Einstein summation notation to describe discrete Fourier transforms on a given axis i.e.

$$\tilde{\rho}_{\tilde{i}} = F_{\tilde{i}i}\rho_i \equiv \sum_i \Delta x\, e^{-ik_{\tilde{i}}x_i}\rho_i \tag{A.2}$$

$$\tilde{\rho}_{\tilde{i}} = F^{-1}_{\tilde{i}i}\rho_i \equiv \sum_i \Delta x\, e^{ik_{\tilde{i}}x_i}\rho_i \tag{A.3}$$

using this notation we write

$$\tilde{P}_{\tilde{i}\tilde{l}\tilde{j}\tilde{m}\tilde{k}\tilde{n}} \equiv F^{-1}_{\tilde{i}i}F^{-1}_{\tilde{j}j}F^{-1}_{\tilde{k}k}F_{\tilde{l}l}F_{\tilde{m}m}F_{\tilde{n}n}P_{iljmkn} \tag{A.4}$$

The density is given using the generalization of the diagonal

$$\rho_{ijk} = P_{iijjkk} \tag{A.5}$$

we can write the element wise position and momentum updates as

$$\tilde{P}_{iljmkn,t+\Delta t} = \tilde{P}_{iljmkn,t}\exp\left[\frac{i\,\Delta t}{2\,m\,\hbar}(p^2_{ijk} - p^2_{lmn})\right]$$
$$P_{iljmkn,t+\Delta t} = P_{iljmkn,t}\exp\left[\frac{i\,\Delta t}{\hbar}(V_{lmn} - V_{ijk})\right] \tag{A.6}$$

[1] P. K. Shukla and B. Eliasson, Phys. Rev. Lett. **96**, 245001 (2006).
[2] H.-Y. Schive, M.-H. Liao, T.-P. Woo, S. K. Wong, T. Chiueh, T. Broadhurst, and W.-Y. Pauchy Hwang, Physical Review Letters **113** (2014), 10.1103/PhysRevLett.113.261302.
[3] P. Mocz, M. Vogelsberger, V. H. Robles, J. Zavala, M. Boylan-Kolchin, A. Fialkov, and L. Hernquist, Mon. Not. Roy. Astron. Soc. **471**, 4559 (2017), arXiv:1705.05845 [astro-ph.CO].
[4] A. Surez, V. H. Robles, and T. Matos, *Proceedings of 4th International Meeting on Gravitation and Cosmology (MGC 4): Santa Clara, Cuba, June 1-4, 2009*, Astrophys. Space Sci. Proc. **38**, 107 (2014), arXiv:1302.0903 [astro-ph.CO].
[5] H.-Y. Schive, T. Chiueh, and T. Broadhurst, Nature Phys. **10**, 496 (2014), arXiv:1406.6586 [astro-ph.GA].
[6] W. Hu, R. Barkana, and A. Gruzinov, Phys. Rev. Lett. **85**, 1158 (2000), arXiv:astro-ph/0003365 [astro-ph].
[7] G. Davies and L. M. Widrow, The Astrophysical Journal **485**, 484 (1997).
[8] D. G. Levkov, A. G. Panin, and I. I. Tkachev, Phys. Rev. Lett. **121**, 151301 (2018).
[9] J. Vicens, J. Salvado, and J. Miralda-Escud, (2018), arXiv:1802.10513 [astro-ph.CO].
[10] E. Y. Davies and P. Mocz, (2019), arXiv:1908.04790 [astro-ph.GA].
[11] P. Mocz, L. Lancaster, A. Fialkov, F. Becerra, and P.-H. Chavanis, Phys. Rev. D **97**, 083519 (2018).
[12] D. Anderson, B. Hall, M. Lisak, and M. Marklund, Phys. Rev. E **65**, 046417 (2002).
[13] F. Haas, G. Manfredi, and M. Feix, arXiv e-prints , cond-mat/0203405 (2002), arXiv:cond-mat/0203405 [cond-mat.str-el].
[14] I. Tan, G. L. Snider, L. D. Chang, and E. L. Hu, Journal of Applied Physics **68**, 4071 (1990), https://doi.org/10.1063/1.346245.
[15] M. Kopp, K. Vattis, and C. Skordis, Phys. Rev. D **96**, 123532 (2017), arXiv:1711.00140 [astro-ph.CO].
[16] M. Garny and T. Konstandin, JCAP **1801**, 009 (2018), arXiv:1710.04846 [astro-ph.CO].
[17] L. M. Widrow and N. Kaiser, The Astrophysical Journal **416**, L71 (1993).
[18] C. Uhlemann, M. Kopp, and T. Haugg, Phys. Rev. **D90**, 023517 (2014), arXiv:1403.5567 [astro-ph.CO].
[19] R. Johnston, A. N. Lasenby, and M. P. Hobson, Monthly Notices of the Royal Astronomical Society **402**, 2491 (2010), http://oup.prod.sis.lan/mnras/article-pdf/402/4/2491/4897464/mnras0402-2491.pdf.
[20] E. Tigrak, R. van de Weygaert, and B. J. T. Jones, Journal of Physics: Conference Series **283**, 012039 (2011).
[21] J. Boris, R. Shanny, U. S. O. of Naval Research, and N. R. Laboratory, *Proceedings: Fourth Conference on Numerical Simulation of Plasmas, November 2, 3, 1970* (Naval Research Laboratory, 1972).
[22] V. Nguyen, B. Izrar, P. Bertrand, and G. Baumann, Physics Letters A **83**, 431 (1981).
[23] N.-D. Suh, M. R. Feix, and P. Bertrand, Journal of Computational Physics **94**, 403 (1991).
[24] P. Bertrand, N. van Tuan, M. Gros, B. Izrar, M. Feix, and J. Gutierrez, Journal of Plasma Physics **23**, 401422 (1980).
[25] L. E. Ballentine, *Quantum Mechanics A Modern Developement*.
[26] K. Yoshikawa, N. Yoshida, and M. Umemura, The Astrophysical Journal **762**, 116 (2012).
[27] P. Bertrand, J. Doremus, B. Izrar, V. Nguyen, and M. Feix, Physics Letters A **94**, 415 (1983).
[28] E. Infeld and A. Skorupski, Nuclear Fusion **9**, 25 (1969).
[29] K. Thorne and R. Blandford, *Modern Classical Physics: Optics, Fluids, Plasmas, Elasticity, Relativity, and Statistical Physics* (Princeton University Press, 2017).
[30] O. Hahn, T. Abel, and R. Kaehler, Mon. Not. Roy. Astron. Soc. **434**, 1171 (2013), arXiv:1210.6652 [astro-ph.CO].

[31] J. O. Thurgood and D. Tsiklauri, Journal of Plasma Physics **82**, 905820604 (2016), arXiv:1612.01780 [physics.plasm-ph].